Letter

Screw dislocation dynamics in confinement-induced layering of Yukawa liquids after quenching

Yun-Xuan Zhang, Hao-Wei Hu, Yi-Cheng Zhao, and Lin I*
Department of Physics and Center for Complex Systems, National Central University, Jhongli, Taiwan 32001, Republic of China

(Received 3 July 2023; accepted 20 December 2023; published 17 January 2024)

Screw dislocation filaments (SDFs) with undefined phases and winded around by helical isophase fronts are fundamental topological defects, which can be used for characterizing the disorder of layered solids and unstable traveling waves. Here, we numerically demonstrate the observation of fluctuating SDFs in the transient relaxation of confinement-induced layering of Yukawa liquids after quenching. We classify the generic dynamical behaviors of screw dislocations (SDs) and unravel their topological origins, which are elusive fundamental issues for general layered systems. It is found that the spatiotemporal growth and decay of layer undulation instability causing sequential rupture and reconnection of a stack of layers are the keys for the formation of SD loops or strings of connected SDFs with alternating helicities, and their spatiotemporal fluctuations. The breaking and reconnection of two approaching SDFs with opposite or the same helicities can form two new separated SDFs. This causes an SD loop to be shed from or merged with another SD loop. The total number of SDs decreases and levels off with increasing time from quenching.

DOI: 10.1103/PhysRevResearch.6.L012012

Screw dislocations (SDs) with undefined phases winded around by helical isophase fronts (surfaces or fronts with the same phases) are fundamental filament-like defects. They widely exist in various three-dimensional (3D) systems with layered structures such as solids [1–4] and traveling waves [5–17]. They can be used as singular objects to characterize the structure and/or dynamics of those systems. For example, in addition to SDs in 3D crystals at the microscopic level [1], SDs were recently found in stacks of macroscopic solid layered structures, such as naturally formed biomineralized nacres [2,3] and block-copolymer layers [4]. The former demonstrated the generation and annihilation of SD pairs with opposite topological charges (helicities) in layer growth [2,3]. After the layers have fully grown, SDs in solids mainly remain static with frozen dynamics.

In acoustic and optical waves, SDs (also named acoustic vortices and optical vortices, respectively) can be passively generated through the interference of linear waves with programed phase difference [5–13,17]. In contrast, SDs with unfrozen dynamics can be *spontaneously* generated in unstable nonlinear traveling waves [14–16]. By monitoring the particle density evolution in an xy plane normal to the wave propagation direction, the experiments described in Refs. [14–16] involving self-excited dust acoustic waves demonstrated the spontaneous emergence of chaotic SD filaments (SDFs) in the xyt space. The *temporal* growth of a modulation or kink instability causing waveform undulation, rupture, and reconnection was found to be the key for the spontaneous pair generation of SDFs with opposite helicities [14]. However, the generic dynamical behaviors of SDs remain elusive due to the difficulty of monitoring the waveform evolution in the xyz space under high wave speed.

Liquids under tight confinement are intensively studied fundamental mesoscopic systems, exhibiting rich structural and dynamical behaviors different from bulk liquids [18–35]. Microscopically, the flat confinement boundary suppresses the transverse thermal motion, lines up particles, and causes the formation of layers near the flat boundary, which can be extended inward by cooling [24,27,33,35]. In the transient relaxation after quenching, the evolving layered structure could be associated with layer undulation and mismatches, which possibly allows spontaneous SD formation with unfrozen dynamics.

Nevertheless, regardless of their potential as good candidates for unraveling the generic behaviors of SDs with unfrozen dynamics, previous studies on confined mesoscopic liquids have been mainly from the conventional viewpoint of particle microstructure and motion. Studies of layer formation [18–35], the associated sluggish dynamics [20,27,32], and various 3D crystalline ordered domains in the steady state after deep cooling [32–35] are a few good examples. Nevertheless, little attention has been paid to the rich dynamical behaviors in the transient relaxation after quenching, especially not from the perspective of SDs and their generic dynamical behaviors and topological origins.

Here, using a relaxing 3D Yukawa liquid confined by two parallel flat boundaries after quenching as a platform, we numerically demonstrate spontaneously formed SD filaments (SDFs). By monitoring the evolving stereo layering fronts surrounding SDFs, their generic dynamical behaviors such as SD emergence, shape variation, interaction, and annihilation in the relaxation are classified. Their topological origins are unraveled. The findings should also be generic for other general unstable layered systems.

*Corresponding author: lini@phy.ncu.edu.tw

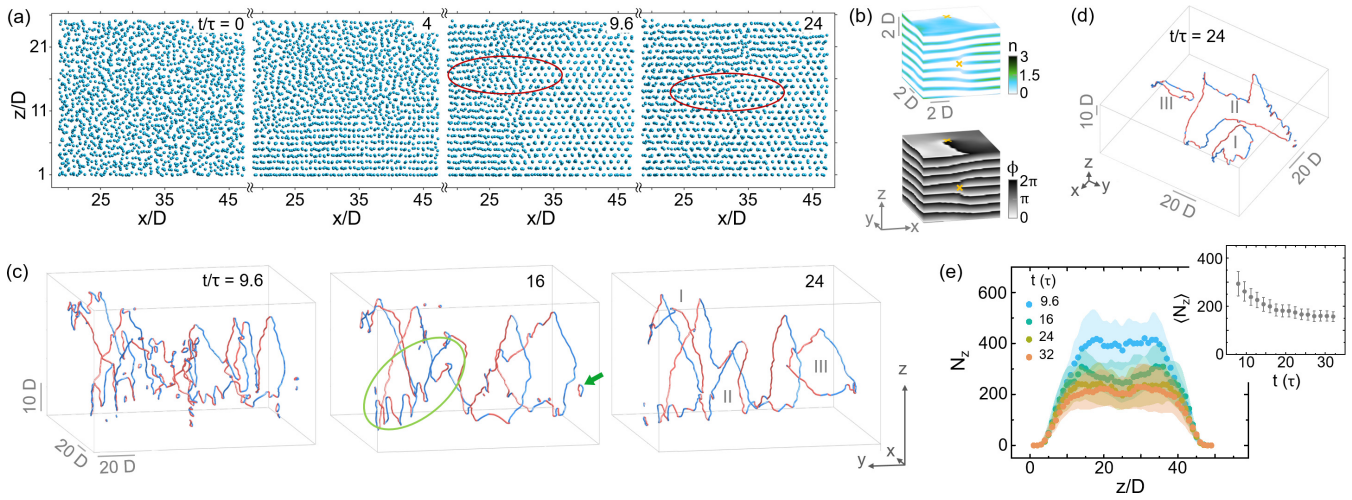

FIG. 1. (a) Side-view snapshots of particle configurations in the lower half of the thin vertical slab (3.5 D in thickness) normal to the boundary, at $t = 0\ \tau$, $4\ \tau$, $9.6\ \tau$, and $24\ \tau$. The first layer is located at $z/D = 1$. The red ellipses highlight the regions without perfect layering alignment. (b) Color-coded plots of particle local density n (top) and the corresponding phase ϕ (bottom) on the xy, xz, and yz planes, at $t = 24\ \tau$. The crosses denote defect locations with undefined phases. (c) Sequential snapshots of SDFs in the entire simulation box. The green arrow indicates the small SD loops. (d) Same plot as that of the SDFs in (c) at $t = 24\ \tau$, but from another viewing angle showing the SDFs in the form of loops (loops I–III). (e) Temporal evolution of the vertical distribution of SD number N_z, with the inset depicting the temporal evolution of the spatial average of N_z over z.

The Langevin-type equations through coupled Yukawa interactions of 524 288 particles are used for our molecular dynamics simulation (see more details in the Supplemental Material (SM) [36]). The system is quenched from the liquid state with temperature $T = 14.33\ T_L$ to $T = 0.95\ T_L$ at time $t = 0$, where T_L is the transition temperature to the state with layering extending over the entire liquid. This allows the formation of 49 layers between two parallel flat confinement plates.

Figure 1(a) shows typical side-view snapshots of particle configurations in the lower half of a thin vertical slab 3.5 D in thickness and normal to the flat boundaries, at different t values, $t = 0\ \tau$, $4\ \tau$, $9.6\ \tau$, and $24\ \tau$, for a typical run after quenching. Here, $\tau = 10^5\ \tau_0$ (see the definition of τ_0 in the SM [36]), and D is the mean interlayer distance, which is $0.87\ a$ (a is the mean separation between two adjacent intralayer particles). Figure 1(a) clearly demonstrates the invasion of the fluctuating layering front from the boundary toward the center. At $t = 9.6\ \tau$, layering fully extends over the entire system, which is the time for accurately identifying SDs. Note that not all the layers are perfectly aligned [e.g., the regions highlighted by ellipses in Fig. 1(a)].

To characterize the local layering order, we further calculate $n(x, y, z)$, the normalized local particle density, by setting the spatiotemporally averaged $n = 1$ (see SM [36]). The top panel of Fig. 1(b) shows the typical stereo snapshot color-coded by n on the xy, xz, and yz surfaces at $t = 24\ \tau$. The center of the front xz plane corresponds to the center of the region highlighted by an ellipse in the rightmost panel of Fig. 1(a). Consistent with the wavy layering pattern in Fig. 1(a), the top panel of Fig. 1(b) demonstrates the wavy pattern with amplitude and phase modulation, as more clearly demonstrated by the plots of the corresponding phase ϕ of n in the bottom panel of Fig. 1(b).

As shown in Fig. 1(b), defects emerge (labeled by crosses) at the vertices of the pitchfork-shaped n pattern, or at the ends of interface lines between the white and the black patches in the xy plane, where the local amplitudes A and phases ϕ of n are null and undefined, respectively (see more details for computing A and ϕ and locating SDs in the SM [36]).

Figure 1(c) shows a few stereo plots of SD configurations in the 3D simulation box ($120\ D \times 120\ D \times 50\ D$) at a few typical t, where SDFs with $+1$ and -1 topological charges are color-coded by blue and red, respectively (see more examples of the SD plots from other runs from the same initial temperature, sequential snapshots showing the temporal evolution of SDFs in the region highlighted by an ellipse, and the charge determination in the SM [36]). Figure 1(d) shows the corresponding stereo SD plot at $t = 24\ \tau$ viewing from another angle.

Basically, SDs appear in the form of chaotic filaments with small-scale wiggling and large-scale zigzag fluctuations, composed of connected SDF segments with alternating topological charges. SDFs can form small loops [e.g., indicated by the arrow in Fig. 1(c)] and large loops [labeled as loops I–III in Fig. 1(d)], or periodic long strings with the same spatial periods as the simulation box width (Fig. S6(c) of the SM [36]). As shown in Fig. 1(c), with increasing t from $9.6\ \tau$ to $24\ \tau$ the small-scale zigzag fluctuations and the small SD loops gradually disappear. From $t = 16\ \tau$ to $t = 24\ \tau$, the system nearly reaches the steady state with only a few large closed SD loops exhibiting small wiggling.

Figure 1(e) shows how N_z, the number of SDs in the xy plane of the entire simulation box at different z, averaged over 13 repeated runs with the same quenching process but different starting microconfigurations, changes with z and t. The plateau-shaped N_z distribution with fast descending tails at both ends indicates the increasing layering order by the

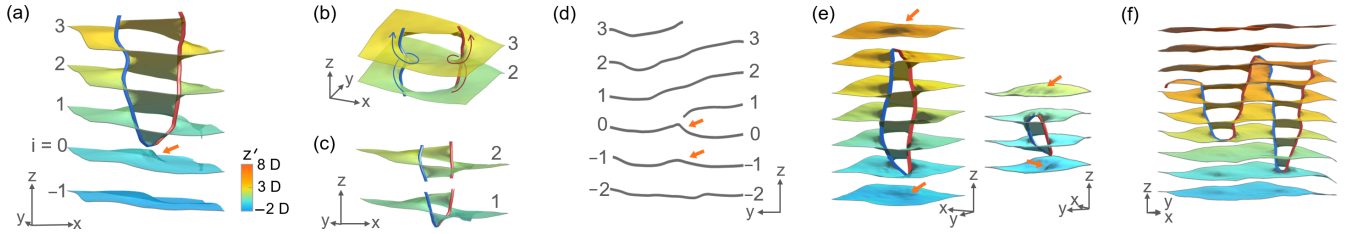

FIG. 2. (a) Stereo plot of layer crest surfaces (isophase surface of $\phi = 0$), color-coded by height z' around a pair of SDFs with opposite charges in the xyz space. (b) and (c) Decomposed plots viewing from different angles. (d) Crest positions in the yz plane normal to and through the center of the surface covering the filament pair shown in (a). (e) Plots showing the O-shaped SD loops composed of SDF pairs and spanning over five (left panel) and two (right panel) layers, and (f) a W-shaped SD string composed of connected SDF segments with alternating charges. The arrows in (a), (d), and (e) indicate the kink locations. The vector lengths of the coordinates equal 1 D and 2 D in the z direction and in the x and y directions, respectively.

increasing confinement effect approaching the confinement boundary. The plateau height exhibits fast initial decay and then levels off with increasing t. The former evidences the gradual inward propagation of layering order from the boundary region, while the latter indicates that highly suppressed thermal agitations after quenching cannot overcome energy landscape barriers to induce SD-free perfect layering in the later stage after quenching. The inset of Fig. 1(e) indicates that $\langle N_z \rangle$, the spatial average of N_z, over z also gradually levels off after the fast initial decay.

What is the 3D layer structure near SDFs? Figure 2(a) shows the isophase surfaces of $\phi = 0$ (corresponding to the crest surfaces of the wavy n patterns in the xyz space) labeled by the layer number i ($i = 0$ is the first layer before the onset of SDF pair generation) and color-coded by height z' ($z' = 0$ is the averaged height of layer 0) surrounding a V-shaped SDF composed of two SDF segments winded around by helical crest surfaces with opposite helicities. Namely, they have opposite topological charges (see SM [36] for the decomposed waveform and charge definition).

How are the SDF segments with opposite charges in the xyz space formed in a pairwise manner? In addition to the plot in Fig. 2(a), this can be more clearly illustrated by Figs. 2(b) and 2(c) showing the decomposed stereo plots of the few crest surfaces viewed from different angles, and Fig. 2(d) showing the crest positions in the yz plane normal to and intersecting the surface covering the two SDF segments in Fig. 2(a). These figures demonstrate that the gradually decreasing confinement effect with increasing normal distance from the boundary facilitates the more easily thermally excited layer undulation instability. This causes the wavy crest pattern and the formation of a local kink indicated by the arrows on surface $i = 0$ in Figs. 2(a) and 2(d). The *spatial* growth of the instability with increasing z causes the sequential rupturing along lines with finite length on the stack of crest surfaces with increasing i. The reconnection of the upward bending part of the ruptured crest i with the downward bending part on the opposite side of the upper crest $i + 1$ [see Fig. 2(c) for a better view] leads to the formation of a pair of SDFs winded around by crest surfaces with opposite helicities and located at the two ends of the ruptured-reconnected lines of crest surfaces, where the phases are not defined.

Note that the above mechanism of the SDF pair generation shares the same topological origin of sequential rupturing and reconnection of isophase surfaces after kink formation due to the *temporal* growth of undulation instability as those found in the xyt space for an unstable 3D plane dust acoustic wave traveling in the z direction [14–16].

As shown in Fig. 2(e), through a reverse process, an SDF can annihilate in a pairwise manner with its own twin sister and form a small vertical O-shaped loop after pair generation. The height of the O-shaped loop can extend from about 1 D to several D. A single SDF segment can also extend apart from its twin sister after pair generation and connect with an SDF segment with an opposite charge from another SDF pair [Fig. 2(f)]. The repeated SDF pair generation-annihilation processes are the keys for the formation of the large-scale crown-shaped (zigzag-shaped) SD loop composed of connected SDF segments with alternating topological charges depicted in Fig. 1, under the conservation of total topological charge.

Now let us focus on the key SDF dynamical processes and their topological origins after pair generation. Figure 3(a) shows an example of the sequential stereo plots of an SDF pair and the surrounding crest surfaces in the xyz space. With increasing t, for the crest below the initial SDF pair tip, the temporal growth of the undulation instability enhances kink formation and causes rupturing of a local region and, in turn, the downward advance of the V-shaped SDF pair. Reversely, the temporal decay of the undulation instability can cause the backward advance of the SDF pair tip (Fig. S6(a) of the SM [36]).

The spatiotemporal growth and decay of the undulation instability lead to the following basic SDF dynamical processes, depicted by the examples of sequential snapshots of SDF configurations. Basically, the shapes and the positions of SDFs fluctuate spatiotemporally under thermal agitation, associated with the fluctuations of the heights of the SDF pair tips and the width between the adjacent SDFs. Figure 3(b) shows that the gradual approach of tips A and B shortens and diminishes the SDF between them. Similarly, the decay of the undulation instability can also shrink or diminish a vertical SD loop composed of two SDF segments with opposite charges (not shown).

Figure 3(c) shows that the horizontal fluctuation of SDF segments can cause necking and pinching of two adjacent SDF segments with opposite charges, followed by their breaking and reconnection. It can induce the detachment of a small SD loop from the cusp region of two connected SDF segments.

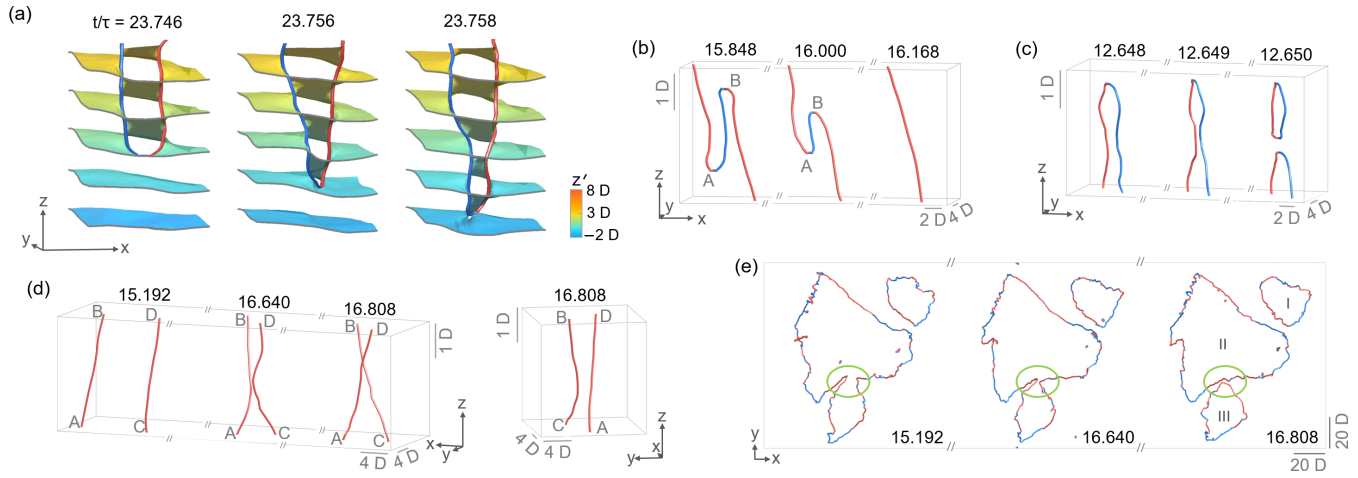

FIG. 3. (a) Sequential plots showing that the temporal growth of kinking-rupture-reconnection instability in the layers below the initial SDF pair tip can lead to the downward advance of the V-shaped SDF pair in the *xyz* space. (b)–(d) Temporal evolution of SDFs in the *xyz* space showing examples of three basic SDF processes: straightening of a zigzag SDF string (b), detachment of an O-shaped loop from a V-shaped SDF string through pinching-breaking-reconnection of two horizontally approaching SDFs with opposite charges (c), and breaking-reconnection of two horizontally approaching SDFs with the same charge (d). In (d), the separation of the two SDFs after reconnection can be better illustrated from another angle, shown in the separate panel at right. (e) Dissociation of a large SD loop into two separated loops (top view) through the process shown in (d) in the region highlighted by ellipses. The vector lengths of the coordinates equal 1 *D* and 4 *D* in the *z* direction and in the *x* and *y* directions, respectively.

Can the two horizontally approaching SDF segments with the same charge also be spontaneously broken and reconnected to form two different separated SDFs? As shown in the sequential snapshots in Fig. 3(d), the two separated SDF segments with ends A-B and C-D, and different tilting angles in the *xyz* space, move toward each other, form a large X, break at the intersection points, and reconnect to form two separated new SDF segments, with ends A-D and C-B (also see the separate panel at right from a different angle).

Figure 3(e) further shows an example of the detachment of a small SDF (loop III) through the same pathway as in Fig. 3(d) after thermally induced SD loop indentation and pinching in the regions highlighted by ellipses in Fig. 3(e).

Note that the processes which are the reverse of the basic processes shown in Fig. 3 have also been observed (see Figs. S6(a)–S6(d) of the SM [36]).

In conclusion, by monitoring the microevolution of confinement-induced layering in a quenched 3D Yukawa liquid numerically, we demonstrated the formation of SDFs and unraveled their transient spatiotemporal relaxation, through classifying their basic dynamical processes and constructing clear micropictures from the stereo particle density waveforms surrounding SDFs. It is found that after layering extending over the entire liquid, SDFs appear in the form of small loops, composed of two SDF segments with opposite charges, and zigzag-shaped larger loops or strings, composed of connected SDF segments with alternating charges. With increasing t, the small-scale spatial fluctuations of SDFs gradually decrease, leaving large SD loops or long SD strings exhibiting slower temporal fluctuations.

The basic dynamical processes of SDFs after pair generation can be classified as follows: (a) The first category is vertical propagation of the cusp formed by two connected SDF segments with opposite charges. This can cause the annihilation of two vertically approaching adjacent cusps, which shrink or diminish a small SD loop, or straighten a zigzag SDF composed of two SDF segments sandwiching a center SDF segment with opposite helicity. (b) The second category involves the breaking and reconnection of two horizontally approaching adjacent SDFs with opposite charges. This process can detach a small vertical SD loop from the SDF cusp tip region. (c) The third category involves the breaking and reconnection of two horizontally approaching SDFs with the same charge; this process splits an indented large SD loop into two separated SD loops. (d) The fourth category includes processes which are the reverse of the processes in categories (a)–(c).

The spatial growth of the undulation instability due to decreasing confinement-induced layering with increasing normal distance to the confinement boundary can cause local kink formation in the layer crest surface, followed by the sequential rupture and reconnection of a stack of trailing crest surfaces. This is the key for the pair generation of SDFs with opposite helicities at the two ends of the rupture-reconnect lines on the crest surfaces in the *xyz* space. The reverse process leads to the approach of an SDF to another conjugate SDF and the annihilation of these two SDFs. Similar rupture and reconnection of crest surfaces through the *temporal* growth and decay of the undulation and kinking instability can cause the vertical and horizontal motion of SDFs, which govern the SDF dynamical processes after SDF pair generation.

Note that regardless of the changes in κ and the gap width, the above SD behaviors are general in the confined liquid after quenching, if the system is ordered enough to allow layering extending to the center region and weakly unstable to such a degree as to allow undulation instability causing layer rupture

and reconnection (see more details in Sec. S6 of the SM [36]).

This work sheds light on and opens another window on understanding and testing the generic behaviors of SDF formation, motion, and interactions for various extended systems with unstable layers or wave fronts. It also provides an alternative perspective from which to understand and characterize the transient dynamics of confinement-induced layering of a liquid after quenching.

This work is supported by the Ministry of Science and Technology of Taiwan, under Contract No. MOST-111-2112-M-008-017.

[1] P. M. Chaikin and T. C. Lubensky, *Principles of Condensed Matter Physics* (Cambridge University Press, Cambridge, 1995), Chap. 9, pp. 495–589.

[2] M. Beliaev, D. Zöllner, A. Pacureanu, P. Zaslansky, and I. Zlotnikov, Dynamics of topological defects and structural synchronization in a forming periodic tissue, Nat. Phys. **17**, 410 (2021).

[3] J. Gim, A. Koch, L. M. Otter, B. H. Savitzky, S. Erland, L. A. Estroff, D. E. Jacob, and R. Hovden, The mesoscale order of nacreous pearls, Proc. Natl. Acad. Sci. USA **118**, e2107477118 (2021).

[4] H. S. Kang, C. Park, H. Eoh, C. E. Lee, D. Y. Ryu, Y. Kang, X. Feng, J. Huh, E. L. Thomas, and C. Park, Visualization of nonsingular defect enabling rapid control of structural color, Sci. Adv. **8**, eabm5120 (2022).

[5] J. F. Nye and M. V. Berry, Dislocations in wave trains, Proc. R. Soc. London, Ser. A **336**, 165 (1974).

[6] B. T. Hefner and P. L. Marston, An acoustical helicoidal wave transducer with applications for the alignment of ultrasonic and underwater systems, J. Acoust. Soc. Am. **106**, 3313 (1999).

[7] J. L. Thomas and R. Marchiano, Pseudo angular momentum and topological charge conservation for nonlinear acoustical vortices, Phys. Rev. Lett. **91**, 244302 (2003).

[8] S. Gspan, A. Meyer, S. Bernet, and M. Ritsch-Marte, Optoacoustic generation of a helicoidal ultrasonic beam, J. Acoust. Soc. Am. **115**, 1142 (2004).

[9] K. Volke-Sepulveda, A. O. Santillan, and R. R. Boullosa, Transfer of angular momentum to matter from acoustical vortices in free space, Phys. Rev. Lett. **100**, 024302 (2008).

[10] R. Marchiano and J. L. Thomas, Doing arithmetic with nonlinear acoustic vortices, Phys. Rev. Lett. **101**, 064301 (2008).

[11] A. M. Yao and M. J. Padgett, Orbital angular momentum: origins, behavior and applications, Adv. Opt. Photonics **3**, 161 (2011).

[12] P. K. Shukla, Twisted dust acoustic waves in dusty plasmas, Phys. Plasmas **19**, 083704 (2012).

[13] E. Hemsing, A. Knyazik, M. Dunning, D. Xiang, A. Marinelli, C. Hast, and J. B. Rosenzweig, Coherent optical vortices from relativistic electron beams, Nat. Phys. **9**, 549 (2013).

[14] Y. Y. Tsai and L. I, Observation of self-excited acoustic vortices in defect-mediated dust acoustic wave turbulence, Phys. Rev. E **90**, 013106 (2014).

[15] Y. Y. Tsai, J. Y. Tsai, and L. I, Generation of acoustic rogue waves in dusty plasmas through three-dimensional particle focusing by distorted waveforms, Nat. Phys. **12**, 573 (2016).

[16] J. Y. Tsai, P. C. Lin, and L. I, Single to multiple acoustic vortex excitations in the transition to defect-mediated dust acoustic wave turbulence, Phys. Rev. E **101**, 023210 (2020).

[17] M. Cromb, G. M. Gibson, E. Toninelli, M. J. Padgett, E. M. Wright, and D. Faccio, Amplification of waves from a rotating body, Nat. Phys. **16**, 1069 (2020).

[18] C. L. Rhykerd, M. Schoen, D. J. Diestler, and J. H. Cushman, Epitaxy in simple classical fluids in micropores and near-solid surfaces, Nature (London) **330**, 461 (1987).

[19] P. A. Thompson, G. S. Grest, and M. O. Robbins, Phase transitions and universal dynamics in confined films, Phys. Rev. Lett. **68**, 3448 (1992).

[20] D. G. Grier and C. A. Murray, The microscopic dynamics of freezing in supercooled colloidal fluids, J. Chem. Phys. **100**, 9088 (1994).

[21] J. Klein and E. Kumacheva, Confinement-induced phase transitions in simple liquids, Science **269**, 816 (1995).

[22] B. Bhushan, J. N. Israelachvili, and U. Landman, Nanotribology: friction, wear and lubrication at the atomic scale, Nature (London) **374**, 607 (1995).

[23] J. Gao, W. D. Luedtke, and U. Landman, Layering transitions and dynamics of confined liquid films, Phys. Rev. Lett. **79**, 705 (1997).

[24] S. Granick, Soft matter in a tight spot, Phys. Today **52**(7), 26 (1999).

[25] M. Zuzic, A. V. Ivlev, J. Goree, G. E. Morfill, H. M. Thomas, H. Rothermel, U. Konopka, R. Sütterlin, and D. D. Goldbeck, Three-dimensional strongly coupled plasma crystal under gravity conditions, Phys. Rev. Lett. **85**, 4064 (2000).

[26] M. Heuberger, M. Zäch, and N. D. Spencer, Density fluctuations under confinement: When is a fluid not a fluid? Science **292**, 905 (2001).

[27] L. W. Teng, P. S. Tu, and L. I, Microscopic observation of confinement-induced layering and slow dynamics of dusty-plasma liquids in narrow channels, Phys. Rev. Lett. **90**, 245004 (2003).

[28] R. Haghgooie and P. S. Doyle, Structure and dynamics of repulsive magnetorheological colloids in two-dimensional channels, Phys. Rev. E **72**, 011405 (2005).

[29] K. Sandomirski, E. Allahyarov, H. Löwen, and S. U. Egelhaaf, Heterogeneous crystallization of hard-sphere colloids near a wall, Soft Matter **7**, 8050 (2011).

[30] L. Chen, C. R. Cao, J. A. Shi, Z. Lu, Y. T. Sun, P. Luo, L. Gu, H. Y. Bai, M. X. Pan, and W. H. Wang, Fast surface dynamics of metallic glass enable superlatticelike nanostructure growth, Phys. Rev. Lett. **118**, 016101 (2017).

[31] S. Arai and H. Tanaka, Surface-assisted single-crystal formation of charged colloids, Nat. Phys. **13**, 503 (2017).

[32] Q. L. Bi, Y. J. Lü, and W. H. Wang, Multiscale relaxation dynamics in ultrathin metallic glass-forming films, Phys. Rev. Lett. **120**, 155501 (2018).

[33] W. Wang, H. W. Hu, and L. I, Surface-induced layering of quenched 3D dusty plasma liquids: Micromotion and structural rearrangement, Phys. Rev. Lett. **124**, 165001 (2020).

[34] Q. Gao, J. Ai, S. Tang, M. Li, Y. Chen, J. Huang, H. Tong, L. Xu, H. Tanaka, and P. Tan, Fast crystal growth at ultra-low temperatures, Nat. Mater. **20**, 1431 (2021).

[35] Y. C. Zhao, H. W. Hu, and L. I, Percolation transitions of confinement-induced layering and intralayer structural orders in three-dimensional Yukawa liquids, Phys. Rev. E **107**, 044119 (2023).

[36] See Supplemental Material at http://link.aps.org/supplemental/10.1103/PhysRevResearch.6.L012012 for (a) the numerical simulation method, (b) the method for identifying screw dislocations, (c) examples of 3D SDF configurations, (d) examples of the stereo structure of layering fronts, (e) dynamical processes of SDF fluctuations that are the reverse of those in Fig. 3, and (f) the generality of SDs in a tightly confined liquid after quenching, as well as the following videos: video S1, which shows the temporal evolution of 3D SDF configurations in the entire simulation box viewing from two different angles, and video 2, which shows the 3D SDF configuration in the entire simulation box viewing from different angles at a fixed time.